Disentangling energetic and charge-carrier dynamic influences on the opencircuit voltage in bulk-heterojunction solar-cells

A. Chelouche, G. Magnifouet, A. Al Ahmad, N. Leclerc, T. Heiser, P. Lévêque

Disentangling energetic and charge-carrier dynamic influences on the open-circuit voltage in bulk-heterojunction solar-cells.

A. Chelouche[1], G. Magnifouet[1], A. Al Ahmad[1], N. Leclerc[2], T. Heiser[1] and P. Lévêque[1*]

[1]Laboratoire des sciences de l'ingénieur, de l'informatique et de l'imagerie (ICube), UMR 7357 Université de Strasbourg-CNRS, 23 rue du Loess, Strasbourg 67037, France.

*E-mail: patrick.leveque@unistra.fr

[2]Institut de Chimie et Procédés pour l'Energie, l'Environnement et la Santé (ICPEES), Département d'Ingénierie Polymère, UMR 7515 Université de Strasbourg-CNRS, 25 rue Becquerel, Strasbourg 67087, France.

Abstract

A combination of transient and static techniques has been applied to bulk-heterojunction solar-cells to gain insight on the influence of charge-carrier dynamics and of energy level shifts in the vicinity of the cathode on the open-circuit voltage. Devices with a different thermal-annealing history but with similar active layer-morphology were compared. P3HT:$PC_{60}BM$ bulk heterojunction solar-cells with a standard ITO/PEDOT:PSS/active-layer/Al were investigated. We show that the open-circuit voltage increase which occurs when a sample is annealed before or after cathode deposition is due roughly one third to a shift between the energetics of the photoactive blend adjacent to the cathode and that in the bulk of the photoactive layer and roughly two thirds to a significant increase in the charge-carrier lifetime for this type of solar-cells.

I. Introduction

In crystalline silicon solar-cells, surface recombination is one of the main carrier-loss mechanisms and a careful passivation of the silicon wafer surface is required to achieve high efficiencies.[1] On the other hand, organic bulk heterojunction (BHJ) solar cells have shown, for a couple of years, a remarkable improvement in their power conversion efficiency (PCE), with PCEs over 10% for the best performing cells.[2] However, while active research on the photoactive layer is, to a large extent, responsible for this impressive improvement, the basic mechanisms limiting the PCE and in particular the influence of charge-carrier dynamics on the PCE are still not well understood. In particular, the role of surface recombination in organic BHJ solar cells is rarely addressed in the literature and mostly by theoretical modeling.[3] Three recent papers describe experimentally and theoretically the influence of surface recombination on BHJ solar cells performances by changing, in a controlled way, the selectivity of the contacts.[4,5,6] As surface recombination is a non-radiative recombination pathway, J. Reinhardt *et al.*[4] have shown a correlation between a weakly selective contact (and

consequently an enhanced surface recombination rate) and a reduction of the electroluminescence signal and of the open-circuit voltage (V_{oc}) of BHJ solar-cells. Moreover, the reduction of V_{oc} was accompanied by a reduction of the forward current. *U. Würfel et al.*[5] have shown that the introduction of organic molecules with a permanent and accurately oriented dipole between the photoactive layer and the electron contact could increase the V_{oc} of BHJ solar-cells. This experimental observation was explained by a decrease of the effective work-function of the electron collecting contact leading to the accumulation of electrons and the depletion of holes in the vicinity of the electron contact and consequently to a reduced surface recombination. Finally, *S. Wheeler et al.*[6] used a variation of the hole-collecting contact work function (by O_2 plasma treatment of the nickel oxide hole contact) to highlight the influence of surface recombination on the V_{oc} of BHJ solar-cells. All these studies combining experimental results and simulations,[4-6] are based on the modification of one of the collecting contacts work-function, either by the introduction of an intermediate layer between the photoactive layer and the contact[4,5] or by a direct physical treatment on the contact itself.[6]

In the present work, we apply a similar experimental approach to test if a thermal annealing, which is a widely used processing step in the elaboration of BHJ solar-cells, could have an impact on the surface recombination and on the open-circuit voltage (V_{oc}) of BHJ solar-cells. In order to estimate the impact of surface recombination on the performances of BHJ solar cells, we chose the widely investigated poly(3-hexylthiophene):1-(3-methoxycarbonyl)propyl-1-phenyl-[6,6]-methanofullerene (P3HT:PC_{61}BM) active layer and a standard ITO/PEDOT:PSS/active layer/Al architecture. The active layer was deposited in the same conditions and from the same solution to minimize sample to sample variations. Moreover, the Al electron-collecting contact (called cathode in the following) was evaporated on all samples during the same thermal evaporation process. The only difference between samples was the thermal annealing/cathode deposition sequence order. The influence of this sequence on the charge-carrier dynamics is investigated in this work. Charge-carrier dynamics were probed by transient photovoltage (TPV) and charge extraction (CE) using a compact setup allowing the use of these transient techniques inside a glove-box system. Therefore, charge-carrier dynamics could be investigated without any device exposure to ambient air between the different steps of the elaboration process (for instance before or after post-elaboration thermal annealing on the same cell).

II. Experimental procedure

All the devices had a standard architecture: glass/ITO/PEDOT:PSS/active layer/Al. Indium Tin Oxide coated glass substrates with a surface resistance lower than 20 Ω/sq were cleaned sequentially by

ultrasonic treatments in deionized water, acetone and isopropyl alcohol. After an additional cleaning for 30 minutes under ultra-violet generated ozone, a highly conductive polyethylene dioxythiophene:polystyrene-sulphonate PEDOT:PSS was spin coated (4500 rpm: 40 nm) from an aqueous solution and dried for 30 minutes at 120°C in nitrogen filled glove box. A dichlorobenzene P3HT (Solaris) and $PC_{61}BM$ (Solenne BV) solution (1:0.8 weight ratio) with a P3HT concentration of 20 mg/ml was used for all devices. The same spin-coating conditions (1250 rpm 60"; 2000 rpm 120") were used to obtain an active layer thickness of 80 nm. A 120 nm thick aluminum layer was thermally evaporated and used as cathode. The device active area was 12 mm^2, while each sample included 4 independent diodes. Two samples with 8 different diodes for each condition were elaborated and tested to estimate the experimental uncertainty. Current density versus Voltage (J-V) characteristics were measured under darkness and under AM1.5G (100 mW/cm^2) illumination using a Sun 3000 (ABET Technologies) solar simulator. The incident light intensity was changed by the addition of neutral filters. The device spectral response was measured inside the glove-box using a home-made setup using an Oriel 150 W solar simulator, a Jobin Yvon microHR monochromator (5 nm resolution) and a calibrated Si photodiode fitted after a beam-splitter to measure the incident light power for each wavelength band. Transient photovoltage (TPV) and charge extraction (CE) measurements were performed inside the glove box using a home-made setup including a white diode array (Bridgelux; nominal CCT = 5600 K), a green diode and a fast MOS field effect transistor (MOS-FET). Tapping-mode atomic force microscopy (AFM) measurements were performed on a Nanoscope IIIa system commercialized by Veeco®.

The only variable parameter in our device elaboration procedure was the thermal annealing (140°C, 15 minutes) performed either before (samples named TA-before) or after cathode evaporation (samples named TA-after). The samples annealed before cathode evaporation were characterized after cathode evaporation and subsequently annealed again (same conditions) (samples named TA-before+after). Conventional (J-V) measurements under standard AM1.5G conditions (100 mW/cm^2) were performed on all samples as well as (J-V) measurements as a function of light power (from 0.9 to 100 mW/cm^2) and external quantum efficiency (EQE) measurements. Then, all samples were investigated by means of TPV and CE techniques to test the influence of device elaboration on charge-carrier dynamics. AFM was also performed on the same samples to check the influence of device elaboration on the active-layer surface morphology.

III. Results and discussion

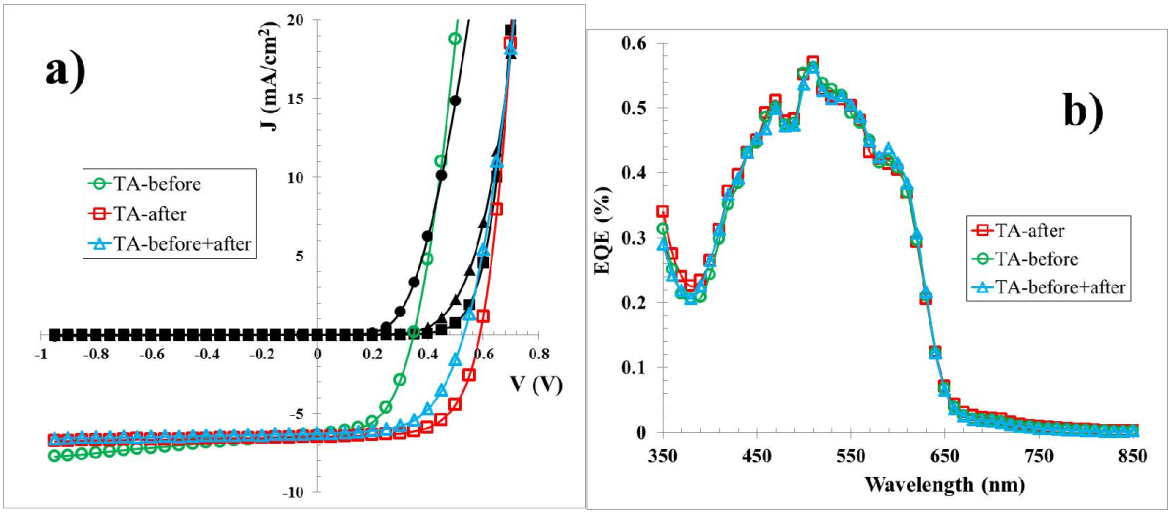

Figure 1: a) (J-V) curves measured in the dark (closed symbols) and under standard AM1.5G illumination (100 mW/cm^2 open symbols) for a diode annealed before cathode deposition (circles), after cathode deposition (squares) and before and after cathode deposition (triangles). b) External quantum efficiency of the different samples.

Representative (J-V) curves for the different types of samples are reproduced in Fig.1a). The average photovoltaic parameters measured on eight different diodes can be found in Table 1. The short-circuit current density (J_{sc}) is almost equal for all the samples while a strong variation in the open-circuit voltage (V_{oc}) with the annealing conditions can be seen.

Table 1: average (uncertainty) photovoltaic parameters measured on different samples.

Sample	J_{sc} (mA/cm^2)	V_{oc} (V)	FF (%)	PCE (%)
TA-before	6.32 (±0.08)	0.35 (±0.09)	53 (±2)	1.2 (±0.2)
TA-after	6.49 (±0.08)	0.59 (±0.03)	64 (±1)	2.44 (±0.05)
TA-before+after	6.27 (±0.07)	0.53 (±0.02)	58 (±2)	1.92 (±0.08)

The samples annealed before cathode deposition show the smallest V_{oc} and the smallest fill factor (FF). The overall power conversion efficiency is rather weak (1.2%). When the samples are annealed after cathode deposition, the V_{oc} is substantially increased (by almost 70%) as well as the FF to reach a PCE more than twice as high. The sample annealed before and after cathode deposition shows a significant improvement in V_{oc} and FF compared to the sample annealed before cathode deposition and approaches the PCE of the sample annealed after cathode deposition. Interestingly, the samples annealed before cathode evaporation show (J-V) curves in the dark and under illumination crossing each other at around 0.45 V while the other samples have a conventional behavior with the illuminated (J-V) curve down shifted by the photo-generated current-density compared to the dark

(J-V) curve (Fig. 1a)), at least in the forward voltage range investigated. The EQE for the three types of samples are almost identical (Fig 1b)). The calculated J_{sc} from the EQE spectra are equal to the measured ones under standard illumination within 5%.

For all types of samples, the photo-generated current-density (estimated as equal to J_{sc} in first approximation) follows an almost linear variation with the incident light intensity in the investigated range. Indeed, as can be seen in Fig. 2a), a power-law variation between J_{ph} and the incident light intensity with a power of 0.9 fits adequately all the measurement points.

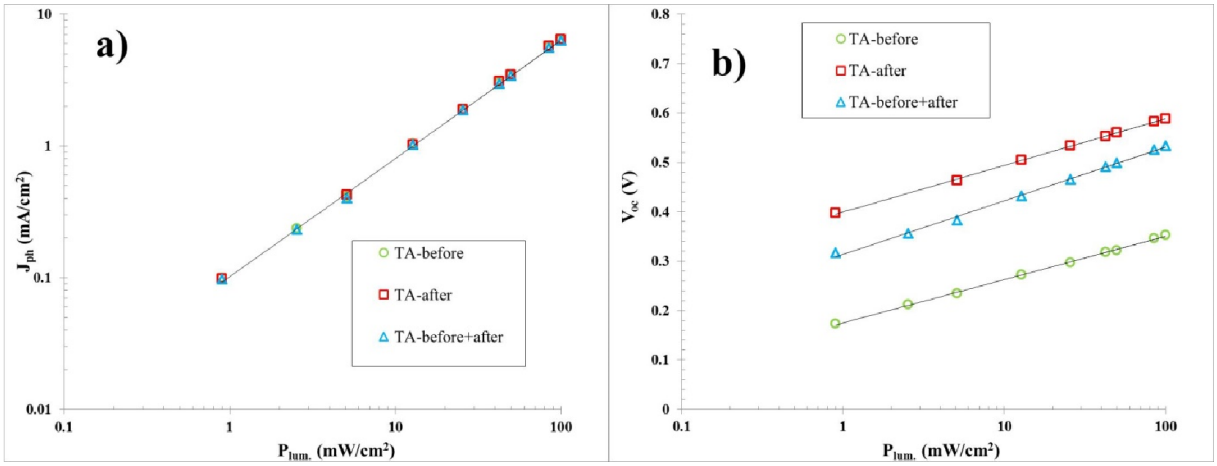

Figure 2: a) photogenerated current-density as a function of light intensity. The line fits all the data with a $J_{ph}=KP_{lum.}^{0.9}$ power law, K being a constant. b) V_{oc} as a function of the light intensity, the lines being fitting exponential laws described by Eq. (2) (coefficient of determination and parameters in Table 2).

Koster *et al.*[7] have shown that for a dominant bimolecular recombination process, the variation of V_{oc} as a function of light intensity could be described by:

$$V_{oc} = \frac{E_g}{q} - \frac{k_B T}{q} Ln\left(\frac{(1-P)\gamma_L N_c^2}{PG}\right) \qquad (1)$$

where E_{gap} is the effective band-gap i.e. the energy difference between the electron-donor (P3HT) HOMO and the electron-acceptor ($PC_{61}BM$) LUMO, q the elementary charge, k_B the Boltzmann constant, T the temperature (K), P the dissociation probability of a bound electron-hole pair, G the generation rate of bound electron-hole pairs, γ_L the Langevin recombination constant and N_c the effective density of states. As G is the only variable depending on light intensity, Eq (1) could be rewritten as:

$$V_{oc} = A + B\frac{k_B T}{q} Ln(P_{lum.}) \qquad (2)$$

where A is not depending on the light intensity, B is equal to one for pure bimolecular recombinations and $P_{lum.}$ is the light intensity. As seen in Fig. 2b), V_{oc} obeys equation (1) but with B being equal to 1.52 (TA-before), 1.64 (TA-after) and 1.88 (TA-after+before). This deviation from B=1 has already been observed in P3HT:PC_{61}BM solar cells and attributed to a trap-assisted recombination process being present in such BHJ solar cells.[8] On the other hand, the substantial variations of A and B as a function of the sample type is quite puzzling. Indeed, the only difference between the samples (TA-before) and (TA-after) is if the thermal-annealing has been performed before or after cathode deposition. The bulk of the photoactive layer is not supposed to be influenced by this sequence order (see AFM images in Fig.5). Therefore, if the bulk morphology is dominating both the charge-carrier generation (bound electron-hole pair generation and dissociation) and recombination (geminate and non-geminate recombination), the same variation of V_{oc} as a function of the light intensity could be expected for both samples. This is obviously not the case and it needs to be further investigated.

Table 2: A and B calculated for the different samples using Eq (2) and Fig. 2 as well as the coefficient of determination R^2.

Sample	A (V)	B	R^2
TA-before	0.17	1.52	0.9991
TA-after	0.40	1.64	0.9995
TA-before+after	0.31	1.88	0.997

TPV has been used on every type of device to gain insight on the influence of the sample history on the charge-carrier dynamics. The V_{oc} is provided by the light intensity of an array of white LEDs while an extra ΔV_{oc} arises from a pulsed green LED with ΔV_{oc} smaller than 5% of V_{oc} to be within the small perturbation regime. Then we measure

$$V_{oc} = V_{oc} + \Delta V_{oc} e^{-\left(\frac{t}{\tau_{\Delta n}}\right)} \qquad (3)$$

and the charge-carrier recombination time $\tau_{\Delta n}$ in the small perturbation regime follows equation (4):

$$\tau_{\Delta n} = \tau_{\Delta n0} e^{-\beta V_{oc}} \qquad (4)$$

similar to previous experimental observations on comparable BHJ solar-cells.[9] The variation of $\tau_{\Delta n}$ as a function of V_{oc} can be found in Fig. 3a) and the fitting parameters using equation (4) in Table 3.

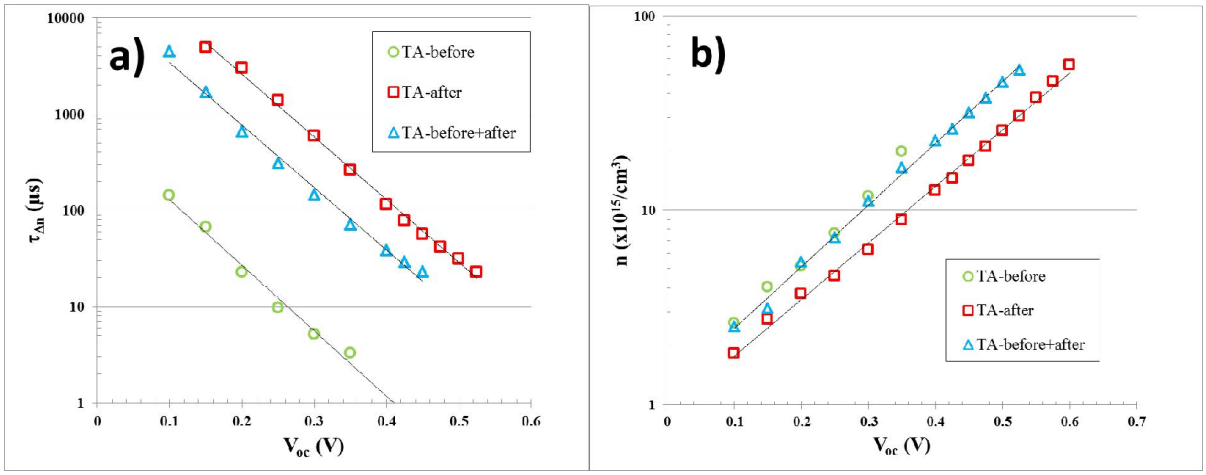

Figure 3: a) variation of the small-perturbation regime charge-carrier recombination time $\tau_{\Delta n}$ as a function of V_{oc}. The lines represent the best fits using Eq. (4) with the parameters of Table 3. b) charge-carrier concentration n as a function of V_{oc}. The lines represent the best fits using Eq. (5) with the parameters of Table 3.

While the β values are close to previously published ones ($\beta \approx 16$ in Ref.9) and do not vary significantly from one sample to the other, the intercept at V_{oc} = 0 V or $\tau_{\Delta no}$ varies from 610 µs (TA-before) to more than 5x10^4 µs (TA-after). Consequently, for a given open-circuit voltage, the charge-carrier recombination time is 20 times higher in the (TA-before+after) sample than in the (TA-before) sample and 80 times higher in the (TA-after) sample than in the (TA-before) sample.

CE has been used on every sample using a white-light pulse of long enough duration to reach the same charge-carrier concentration n than in the corresponding TPV experiments. A fast switching MOS-FET was used to extract those carriers in short-circuit conditions. The n values were corrected to account for the charges accumulated on the electrodes.[10] n follows the generally observed variation as a function of V_{oc} obeying (Fig. 3b):

$$n = n_0 e^{\gamma V_{oc}} \qquad (5)$$

with the fitting parameters given in Table 3. For all the samples, n_0 is in the 1x10^{15}/cm^3 range while γ slightly varies from 6.7 V^{-1} for (TA-after) to 7.3 V^{-1} for the other annealing conditions.

Table 3: fitting parameters obtained for the different samples using Eq. (4) and Eq. (5).

Sample	$\tau_{\Delta no}$ (µs)	β (V^{-1})	n_0 (/cm^3)	γ (V^{-1})	β/γ
TA-before	613	15.6	1x10^{15}	7.3	2.1
TA-after	5.2x10^4	15.0	9x10^{14}	6.7	2.2
TA-before+after	1.5x10^4	14.9	1x10^{15}	7.3	2.0

Combining Fig. 3a) and Fig. 3b) (and Eqs. (4) and (5)) allows to derive the variation of $\tau_{\Delta n}$ as a function of n for every sample. As expected, $\tau_{\Delta n}$ as a function of n can be described by Eq. (6) (Fig. 4):

$$\tau_{\Delta n} = \tau_{\Delta no}\left(\frac{n_0}{n}\right)^{\frac{\beta}{\gamma}} \qquad (6)$$

where β/γ is almost constant for every sample history and equals 2 as already observed for P3HT:PC_{61}BM BHJ solar cells.[9]

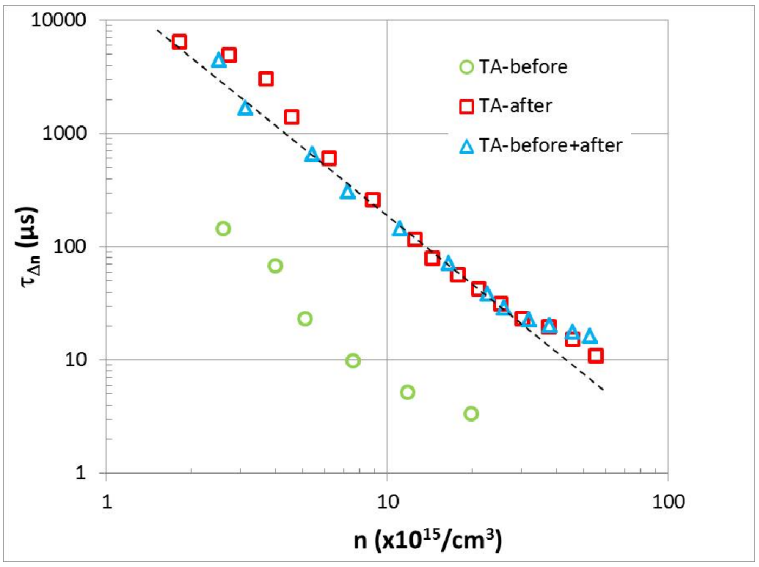

Figure 4: variation of the small-perturbation regime charge-carrier recombination time $\tau_{\Delta n}$ as a function of the charge-carrier concentration n. The dotted line represents a β/γ coefficient equal to 2 (Eq. (6)).

The total charge-carrier population dynamics follows:[9,11,3]

$$\frac{dn}{dt} \approx -\frac{n^{1+\frac{\beta}{\gamma}}}{\left(1+\frac{\beta}{\gamma}\right)\tau_{\Delta no} n_0^{\frac{\beta}{\gamma}}} \approx -kn^3 \qquad (7)$$

The charge carrier decay dynamics exhibiting a third order dependence on charge density (Eq. (7)) is often interpreted as a bimolecular recombination process with a carrier-density dependent coefficient k and can be related to an exponential tail of sub-band-gap localized trap states.[12] The present study reveals that the annealing history of the sample has a strong influence on $\tau_{\Delta no}$ with a limited impact on the other parameters of Eq. (7).

Different parameters could induce the observed variations of the charge-carrier dynamics as a function of the sample history. In particular, it is well known that the blend morphology strongly impact the charge-carrier generation and recombination and therefore the overall photovoltaic parameters. We performed therefore AFM measurements in order to estimate the influence of the

sample history on the blend morphology. We could not probe by AFM the morphology under the contacts. On the other hand, annealing the samples before or after cathode deposition has no noticeable effect on the surface morphology outside the cathode contact (Fig. 5). The extra post-deposition annealing at 140°C for 15 minutes (TA-before+after) has only a minor impact on the phase-separation observed by AFM (Fig. 5). Therefore, even if it has been shown that the top-interface has an impact on the vertical gradient of P3HT and $PC_{61}BM$,[13] we may conclude that the blend morphology and therefore the charge-carrier generation and recombination process in the bulk are only weakly affected by the sample annealing history. Following this hypothesis, the main factor responsible for the variations observed in charge-carrier dynamics appears to be the annealing of the active layer/cathode (Al) interface.

A recent publication by S. Wheeler *et al.*[6] combining transient measurements with device simulations allows us to rationalize the present experimental results. Varying the electrode work-function in their simulations, all the other parameters being unchanged, they observed a shift in V_{oc} for a given charge-carrier density, in accordance with our observation. Indeed, comparing (TA-before) and (TA-before+after) samples with the (TA-after) sample (Fig. 3b)), it can be seen that for the higher charge-carrier density (corresponding roughly to 1 sun illumination), a 70 mV increase in V_{oc} is observed for the (TA-after) sample. This increase in V_{oc} is accompanied by a decrease in the slope (see γ value in Table 3) for the (TA-after) sample as observed in the simulations in Ref. 6.

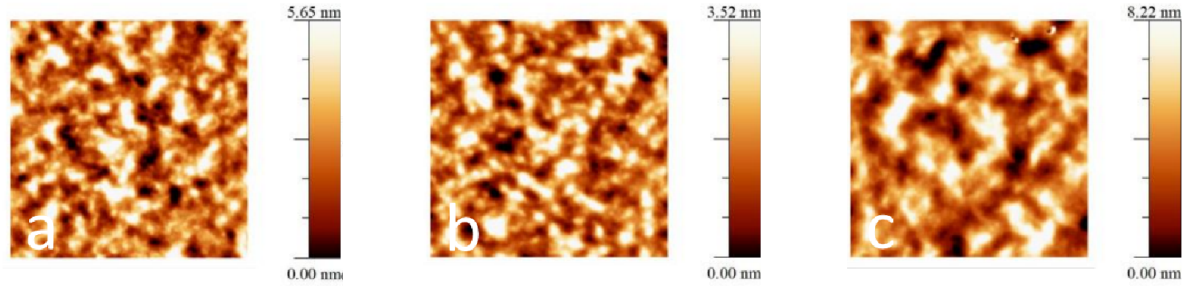

Figure 5: AFM topography image (5x5 µm) of a) TA-before sample, b) TA-after sample and c) TA-before+after sample.

It seems therefore that a change in the cathode work-function may at least partly explain our experimental results in Fig. 3b). In Ref. 6, S. Wheeler *et al.* used an oxygen plasma treatment to vary experimentally the work-function of the nickel oxide hole-transport layer. In the present study, a mild thermal annealing can hardly explain a variation of the work-function of the Al electron-collecting electrode. On the other hand, a mild thermal annealing could induce the formation of an intermixed layer between the cathode and the photoactive layer just underneath and therefore a

difference in the energetics between the photoactive blend adjacent to the cathode and that in the bulk of the device. This could have the same impact as the one observed by *S. Wheeler et al.* i.e. an improved selectivity of the cathode (in our case) and consequently an increased V_{oc} when the sample has been annealed after cathode deposition (TA-after) compared to when the sample has been annealed before cathode deposition (TA-before). Such a hypothesis is consistent with the difference of 70 mV in V_{oc} in static AM1.5G (100 mW/cm^2) photovoltaic measurements between the (TA-before+after) sample (V_{oc} = 0.53 V) and the (TA-after) sample (V_{oc} = 0.59 V). It should be noticed however that a subsequent thermal annealing (TA-before+after) does not produce the same effect as the dependences of n on V_{oc} are similar for (TA-before) and (TA-before+after). Thus, no variation between the photoactive blend adjacent to the cathode and that in the bulk of the device is expected between both types of samples, despite the fact that the measured V_{oc} under standard illumination conditions is much lower for the sample (TA-before) (V_{oc} = 0.35 V) than for the sample (TA-before+after) (V_{oc} = 0.53 V).

As already described in the literature,[14] V_{oc} can be expressed by the difference between an energetic component and a kinetic one:

$$V_{oc} = \frac{1}{q}(IP_D - EA_A) - \frac{n_{id}k_BT}{q} Ln\left(\frac{J_{BI}}{J_{gen}}\right) \qquad (8)$$

where IP_D is the ionization potential of P3HT, EA_A the electron affinity of $PC_{61}BM$ (or the energetics of the contacts or at the vicinity of the contacts), n_{id} the ideality factor, J_{BI} the loss current-density due to non-geminate recombination as measured with TPV and CE and J_{gen} the photo-generated current-density (or J_{sc} in this model). According to Fig. 4, the charge-carrier lifetime for both (TA-after) and (TA-before+after) samples is significantly larger than for the (TA-before) device. At n = 1x10^{16}/cm^3, the lifetime is more than 20 times lower in the sample only annealed before cathode deposition. The ideality factor can be extracted from:[6]

$$n_{id} = \frac{q}{k_BT}\frac{dV_{oc}}{dLn(P_{lum.})} \qquad (9)$$

where $P_{lum.}$ is the light intensity as in Fig. 2b). In a first approximation, the ideality factor is almost constant as a function of the light power and it can be approximated by B (Eq. (2)). The V_{oc} kinetic component described by Eq. (8) going from (TA-before+after) to (TA-before) with a 20 time decrease in $\tau_{\Delta n}$ will lead to a ΔV_{oc} decrease given by:

$$\Delta V_{oc} \approx \frac{n_{id}k_BT}{q} Ln(20) = 150\ mV \qquad (10)$$

quite consistent with the observed V_{oc} decrease under standard illumination from (TA-before+after) (V_{oc} = 0.53 V) to (TA-before) (V_{oc} = 0.35 V).

IV. Conclusions

In conclusion, we measured the charge-carrier dynamics in bulk-heterojunction solar-cells using transient photovoltage (TPV) and charge extraction (CE). We used the same architecture (ITO/PEDOT:PSS/active layer/Al) with the same active layer (P3HT:PC_{61}BM), the same active layer thickness in order to focus on the annealing history of the sample. The BHJ solar cells were either annealed before the Al-cathode deposition, or after cathode deposition. Using the results obtained on a model developed to quantify the influence of surface recombination on charge-carrier kinetics in BHJ solar-cells,[6] it turns out that:

- when the thermal annealing is performed only after the Al-cathode deposition, there is a shift between the energetics of the photoactive blend adjacent to the cathode and that in the bulk of the photoactive layer probably due to the formation of an intermixed layer underneath the cathode. This intermixed layer may improve the selectivity of the cathode as observed in CE measurements with, as a consequence, a V_{oc} increase of 70 mV in the sample annealed only after cathode deposition. On the other hand, no such shift is observed between samples annealed before cathode deposition or before and after cathode deposition. The measured V_{oc} shift using a transient technique is consistent with the static standard photovoltaic measurements where the V_{oc} is increased by roughly 70 mV in samples annealed after cathode deposition compared to samples annealed before and after cathode deposition.
- When the thermal annealing is performed only before the Al-deposition, there is a significant decrease in charge-carrier lifetime (by a factor of 20) that is sufficient to explain the V_{oc} increase (180 mV) between the samples annealed before cathode evaporation and the ones annealed before and after cathode evaporation.
- The observed V_{oc} increase (240 mV) between the samples annealed only before and the samples annealed only after cathode deposition is then a combination of energy level difference between the bulk of the active layer and the interface between the active layer and the cathode (for 70 mV or less than one third) and a significant increase of the charge-carrier lifetime (for 150 mV or almost two thirds).

The combination of transient and static measurement techniques helps to understand and to quantify the complex role of a thermal annealing on BHJ solar cells with comparable active-layer

morphology, both on the energetic and on the kinetic contribution of surface recombination on the open-circuit voltage.

Acknowledgments.

P.L. is grateful to P. Knobloch for the realization of the TPV/CE electronic module. P.L. acknowledge the reviewers for their valuable comments.

[1] A.G. Aberle, *Progress in Photovoltaics*, **8**, 473 (2000).
[2] J. Zhao, Y. Li, G. Yang, K. Jiang, H. Lin, H. Ade, W. Ma and H. Yan, *Nature Energy*, **1**, 15027 (2016).
[3] (a) T. Kirchartz and J. Nelson, *Phys. Rev. B*, **86**, 165201 (2012), (b) S. Schafer, A. Petersen, T.A. Wagner, R. Kniprath, D. Lingenfelser, A. Zen, T. Kirchartz, B. Zimmermann, U. Wurfel, X.J. Feng and T. Mayer, *Phys. Rev. B,* **83**, 165311 (2011), (c) T. Kirchartz, B.E. Pieters, K. Taretto and U. Rau, *Phys. Rev. B*, **80**, 035334 (2009), (d) J.C. Scott and G.G. Malliaras, *Chem. Phys. Lett.* **299**, 115 (1999), (e) T. Kirchartz, B.E. Pieters, K. Taretto and U. Rau, *J. Appl. Phys.* **104**, 094513 (2008).
[4] J. Reinhardt, M. Grein, C. Bühler, M. Schubert and U. Würfel, *Adv. Energy Mater.* **4**, 1400081 (2014).
[5] U. Würfel, M. Seβler, M. Unmüssig, N. Hofmann, M. List, E. Mankel, T. Mayer, G. Reiter, J.-L. Bubendorff, L. Simon and M. Kohlstädt, *Adv. Energy Mater.* **6**, 1600594 (2016).
[6] S. Wheeler, F. Deledalle, N. Tokmoldin, T. Kirchartz, J. Nelson and J.R. Durrant, *Phys. Rev. Applied* **4**, 02420 (2015).
[7] L.J.A. Koster, V.D. Mihailetchi, R. Ramaker and P.W.M. Blom, *Appl. Phys. Lett.* **86**, 123509 (2005).
[8] G-J.A.H. Wetzelaer, M. Kuik and P.W.M. Blom, *Adv. Energy Mater.* **2**, 1232 (2012).
[9] C.G. Shuttle, B. O'Regan, A.M. Ballantyne, J. Nelson, D.D.C. Bradley, J. de Mello and J.R. Durrant, *Appl. Phys. Lett.* **92**, 093311 (2008).
[10] C.G. Shuttle, A. Maurano, R. Hamilton, B. O'Regan, J.C. de Mello and J.R. Durrant, *Appl. Phys. Lett.* **93**, 183501 (2008).
[11] B.C. O'Regan, J.R. Durrant, P.M. Sommerling and N.J. Bakker, *J. Phys. Chem. C* **111**, 14001 (2007).
[12] J. Nelson, *Phys. Rev. B* **67**, 155209 (2003).
[13] M. Campoy-Quiles, T. Ferenczi, T. Agostinelli, P.G. Etchegoin, Y. Kim, T.D.Anthopoulos, P.N. Stavrinou, D.D.C. Bradley and J. Nelson, *Nature Mater.* **7**, 164 (2008).
[14] D. Credington and J.R. Durrant, *J. Phys. Chem. Lett.* **3**, 1465 (2012).